# Synthesis of hierarchical Cd-Ni-MOF micro/nanostructures and derived Cd-Ni-MOF/CdS/NiS hybrid photocatalysts for efficient photocatalytic hydrogen evolution

# Supplementary Information

## Experiment

## Catalysts characterization

The morphology of the as-prepared samples was characterized by scanning electron microscopy (SEM, TESCAN MIRA3 LMH) and transmission electron microscopy (TEM, JEOL JEM-2010) using an accelerating voltage of 200 kV. The X-ray diffraction (XRD) patterns of the samples were obtained on a BRUKER D8 ADVANCE X-ray diffractometer (German) using Cu Ka radiation (λ = 1.5406 Å). The element content of Cd and Ni in Cd-Ni-MOF was determined with the inductively coupled plasma atomic emission spectrometry (Agilent 7800 ICP-MS). X-ray photoelectron spectroscopy (XPS) analysis were performed on a high-resolution Thermo ESCALAB 250 X-ray photoelectron spectrometer (America) with Al (Kα) radiation probe. Photoluminescence (PL) spectra were recorded at room temperature on a fluorescence spectrophotometer (Hitachi F-7000, Japan) using Xenon lamps as the excitation source, all samples were excited to a wavelength of 300 nm. Ultraviolet visible diffuse reflectance spectrometer (PerkinElmer Lambda 750 UV–Vis) is used to measure the light response of the sample. The Brunauer–Emmett–Teller (BET) surface area and the pore size distribution of the catalysts were recorded on a Micromeritics ASAP 2020 M instrument at 77 K. Electron paramagnetic resonance (EPR) of radicals trapped by 5, 5-dimethyl-1-pyrroline N-oxide (DMPO) was determined with a Brucker EPR A 200W spectrometer.

## Photocatalytic $H_2$ evolution and photoelectrochemical experiment

The photocatalytic hydrogen production experiments were carried out under the irradiation of a 300W xenon lamp. Using lactic acid as a sacrificial agent, 10 mg of the photocatalyst was dispersed in 60 mL of a 6 vol% aqueous lactic acid solution. Continuous stirring was used throughout the reaction to avoid catalyst deposition, and cooling water was circulated to keep the system at 7 °C. The reactor was filled with argon to ensure that the system was free of other gases. Hydrogen production was determined using an equipped on-line Agilent GC-950 gas chromatograph. After photocatalytic reaction under visible light irradiation, the solution was centrifuged at 8000 rpm for 10 minutes, washed with ethanol to remove impurities, and vacuum dried at 60°C to obtain the reacted photocatalyst. Stability testing was performed for five cycles of 3 hours each. After each cycle, the atmosphere in the system was replaced with argon.

Photoelectrochemical measurements were conducted on an electrochemical workstation

(Metrohm Autolab; Nova, Altham, MA, USA) with a standard three-electrode cell. The fluorine-doped tin oxide (FTO) electrode (2 × 2 $cm^2$) with drop-coated samples, Saturated calomel electrode (SCE), and platinum electrode were used as working electrode, reference electrode, and counter electrode, respectively. To prepare the FTO working electrode, 5 mg of the sample was dispersed in a mixture of 50 μL Nafion solution and 500 μL ethanol solution by ultrasound to obtain a slurry. Then, the slurry was immersed in pre-protected FTO glass with paper tape at the border. After air drying, the paper tape was removed to obtain a working electrode. All electrochemical measurements were performed in 0.2 M aqueous $Na_2SO_4$ using a 300 W xenon lamp as the light source. The photoelectrochemical experiment contain the transient photocurrent spectroscopy (I–t, photocurrent at 0.598 V vs. SCE), Electrochemical impedance spectroscopy (EIS, 0.2 V potential with SCE) and polarization tests (LSV, -0.5 to 0 V with SCE).

## Mott–Schottky experiments

The efficient charge carrier separation and electron mobility from CdS to Cd-Ni-MOF-T was validated through estimation of the flat band potential and charge carrier density by Mott–Schottky analyses. Space charge capacitance ($1/C_{sc}^2$) vs applied potential curves were obtained under dark conditions at 20 mV $s^{-1}$ over a potential window in which the capacitive current was only observed by cyclic voltammetry. For both CdS and Cd-Ni-MOF-T, a positive–shaped linear tendency was obtained, indicating the n–type semiconductor of each material. According to semiconductor type of both materials, an n–n heterojunction was established and the Mott–Schottky relationship was used to estimate the flat band potential and donor density, as described the Eq. (1):

$$\frac{1}{C_{sc}^2} = \left[\frac{2}{N_d A^2 q \varepsilon \varepsilon_0}\right]\left[E_{app} - E_{fb} - \frac{k_B T}{q}\right]$$

where $N_d$ is the donor density of each photoanodes, A is the exposed geometric area (3 $cm^2$), q is the electron charge, ε is the relative permittivity, $\varepsilon_0$ is the vacuum permittivity, k is the Boltzman constant and T is the absolute temperature in K[1].

## The Figures

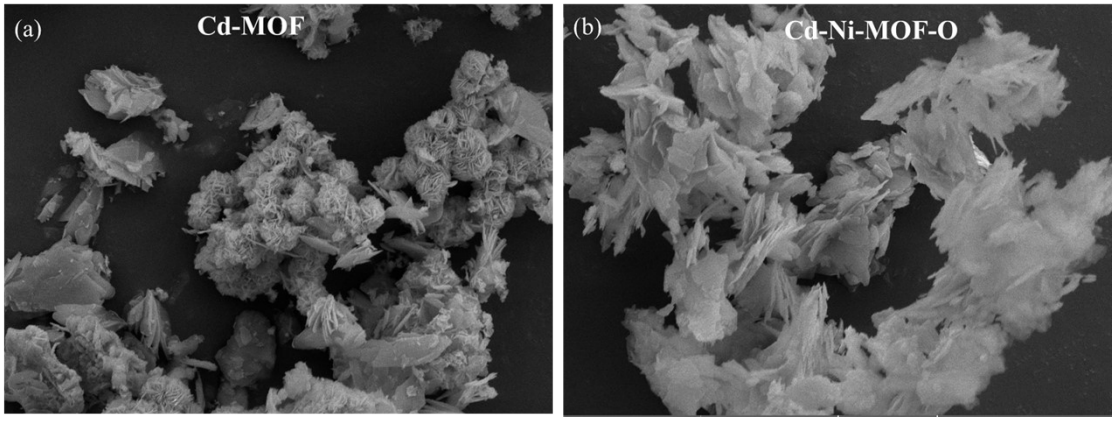


Fig. S1 (a) The SEM images of the Cd-MOF and the as-prepared Cd-Ni-MOF-O sample

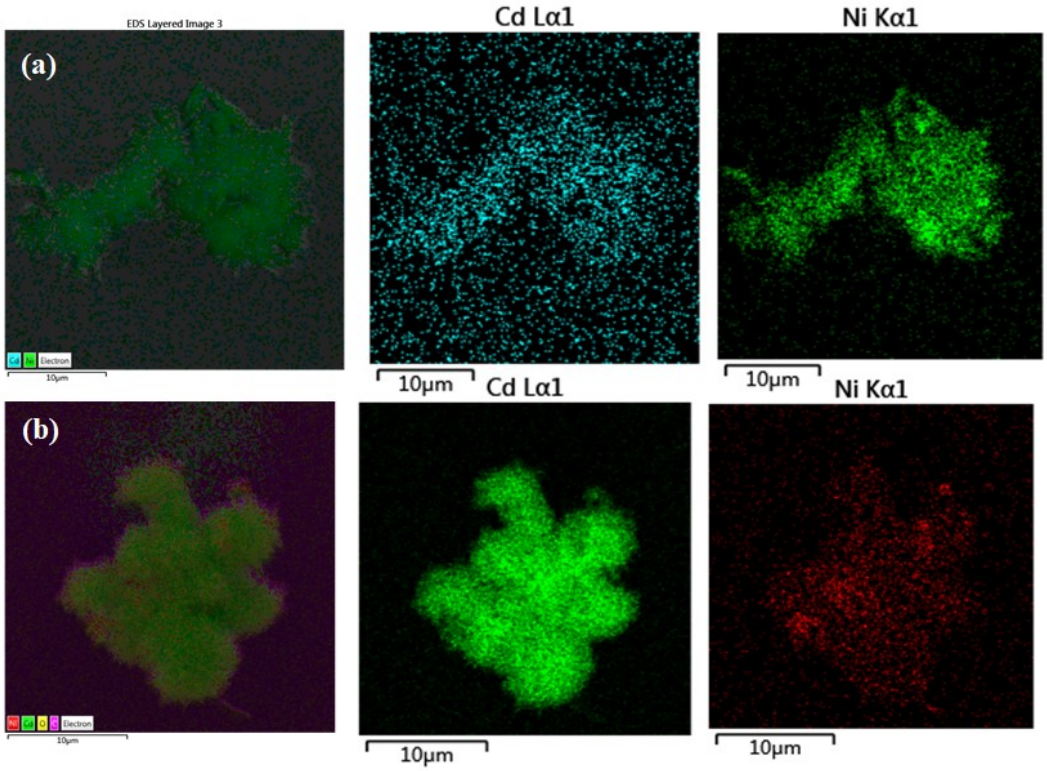


Fig. S2 The SEM-area-Mapping of the Cd-Ni-MOF by one-step(a) and two-step(b) solvothermal process.

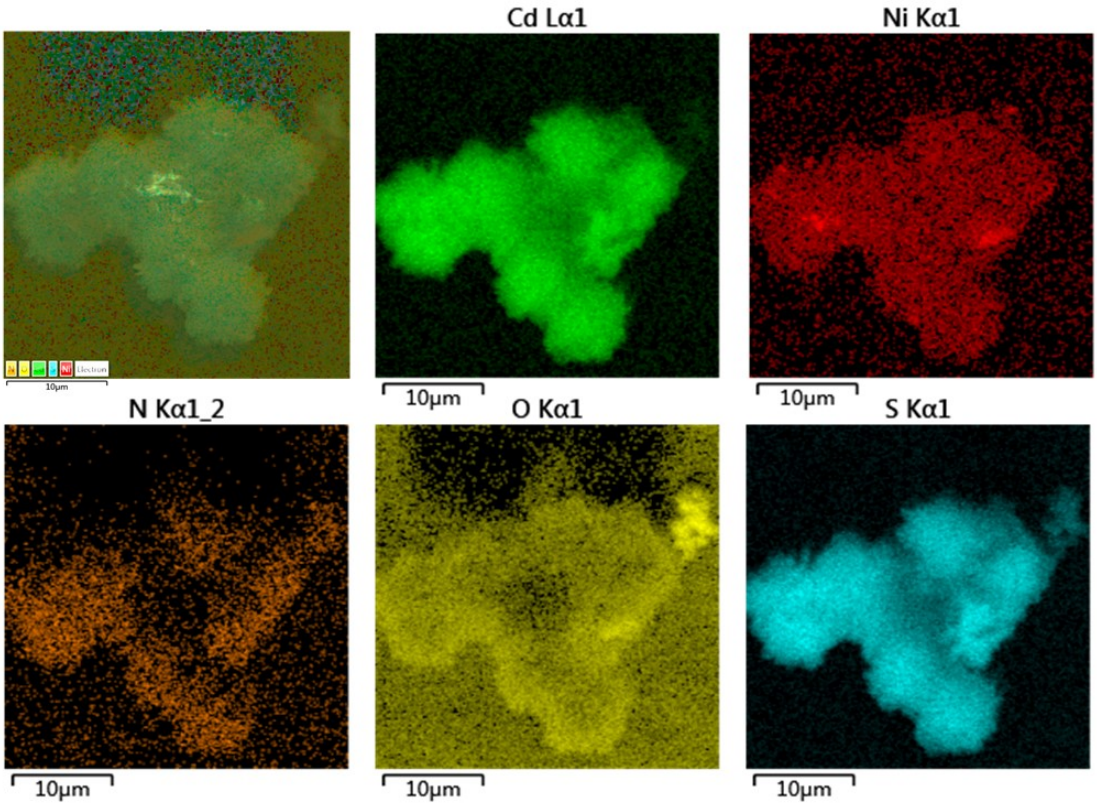


Fig S3 The SEM-area-Mapping of a typically mixed sulfides prepared from the Cd-Ni-MOF-T in 1:1 (v/v) dimethylformamide (DMF) and ethanol solution

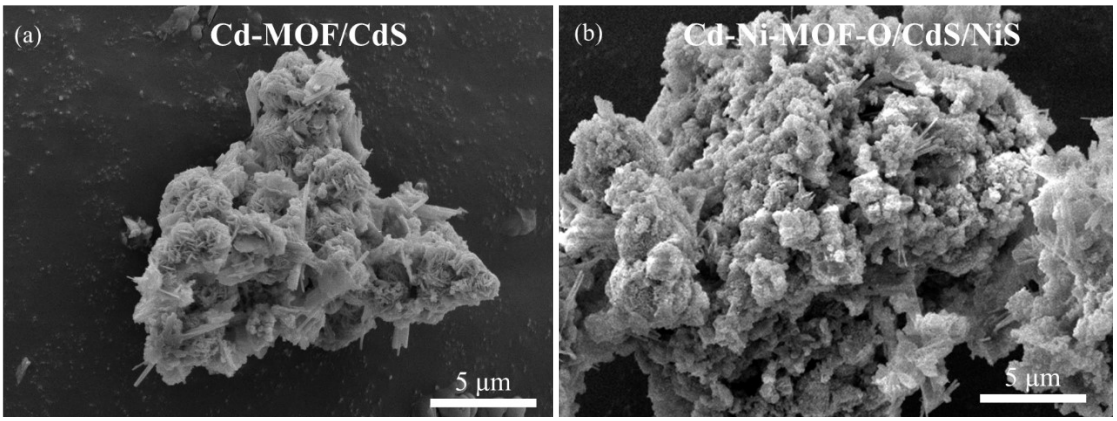


Fig. S4 The SEM of as-prepared sulfides based on the Cd-MOF(a) and one-step synthesized Cd-Ni-MOF-O samples(b)

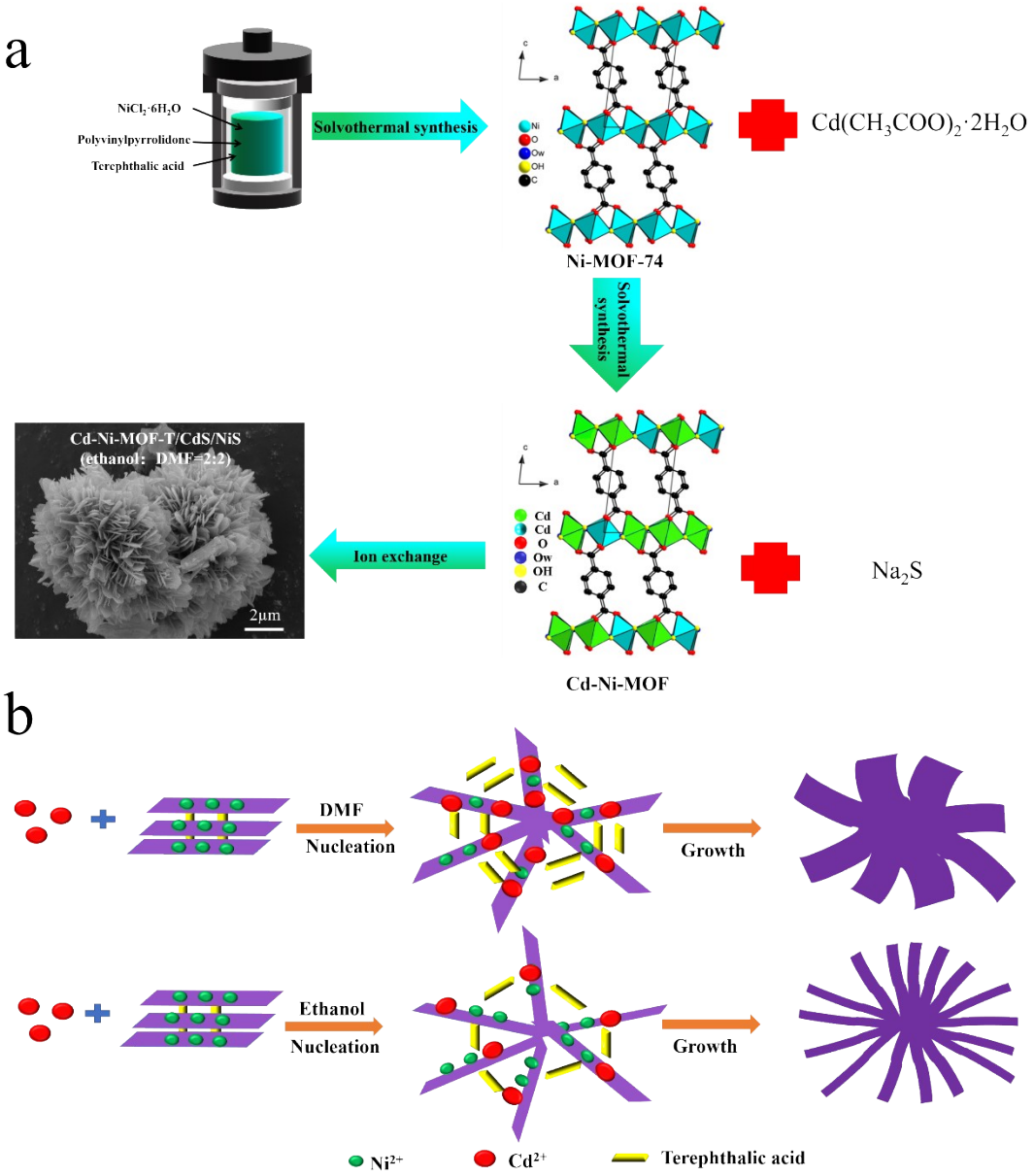


Fig. S5 (a) the synthesis strategy of Cd-Ni-MOF derived sulfides photocatalysts, (b) the possible formative mechanism of different Cd-Ni-MOF structures

Table 1 The related comparsition for produce $H_2$

| Photocatalyst | Production rate | Light source | Reference |
|---|---|---|---|
| CdS/NM(15) | 1.04mmol $g^{-1}$ $h^{-1}$ | 300 W Xe | [2] |
| g-$C_3N_4$– CdS–NiS | 2.56mmol $g^{-1}$ $h^{-1}$ | 300 W Xe | [3] |
| α,β-NiS/CdS/$NH_2$-UiO-66 | 17.88mmol $g^{-1}$ $h^{-1}$ | 300 W Xe | [4] |
| CdS/NiS | 18.10mmol $g^{-1}$ $h^{-1}$ | 300 W Xe | [5] |
| Cd-Ni-MOF-T/CdS/NiS | 40.08mmol $g^{-1}$ $h^{-1}$ | 300 W Xe | Here |
| CdS@NiS | 42.76mmol $g^{-1}$ $h^{-1}$ | 300 W Xe | [6] |

Although some catalysts have hydrogen production performance of 42.76mmol/h, their catalyst morphology has not been adjusted in terms of morphology. We adjusted the morphology of the catalyst and found the unique morphology of MOF. In addition, we found that Cd-Ni-MOF could not be completely cleaned and retained in the structure, which played an important role in maintaining the close contact between CdS and NiS and the subsequent photocatalytic hydrogen production activity.

# Reference


1. Hoyos L. J.; Rivera D. F.; Gualdrón-Reyes A. F.; Ospina R.; Rodríguez-Pereira J.; Ropero-Vega, J. L.; Niño-Gómez, M. E., Influence of immersion cycles during n–β–$Bi_2O_3$ sensitization on the photoelectrochemical behaviour of N-F-codoped $TiO_2$ nanotubes. *Applied Surface Science* **2017,** *423*, 917-926.

2. Niu L.; Zhang, W.G.; Li, H.T.; Wang, H.X.; Wang, J.; Liu, Y.M., The construction of double type II heterostructure from CdS and Ni-MOF-74 with two structures and enhanced mechanism of photocatalytic water splitting. *Journal of Materials Science* **2022,** *57*, 5768-5787.

3. Yuan J.; Wen J.; Zhong Y.; Li X.; Fang Y.; Zhang S.; Liu W., Enhanced photocatalytic H2evolution over noble-metal-free NiS cocatalyst modified CdS nanorods/g-$C_3N_4$ heterojunctions. *Journal of Materials Chemistry A* **2015,** *3*, 18244-18255.

4. Zhang H.; Yu Z.; Jiang R.; Hou Y.; Huang J.; Zhu H.; Yang F.; Li M.; Li F.; Ran Q., Metal organic frameworks constructed heterojunction with α-NiS-β-NiS/CdS: The effect of organic-ligand in UiO-66 for charge transfer of photocatalytic hydrogen evolution. *Renewable Energy* **2021,** *168*, 1112-1121.

5. Liu X.; Bie C.; He B.; Zhu B.; Zhang L.; Cheng B., 0D/2D NiS/CdS nanocomposite heterojunction photocatalyst with enhanced photocatalytic $H_2$ evolution activity. *Applied Surface Science* **2021,** *554*.

6. Liu C.; Liu Y.; Xiang Z.; Liu D.; Yang Q., Bimetallic MOF-Derived Sulfides with Heterojunction Interfaces Synthesized for Photocatalytic Hydrogen Evolution. *Industrial & Engineering Chemistry Research* **2021,** *60*, 11439-11449.